

PadChest-GR: A Bilingual Chest X-ray Dataset for Grounded Radiology Report Generation

Daniel Coelho de Castro¹, Aurelia Bustos², Shruthi Bannur¹, Stephanie L. Hyland¹, Kenza Bouzid¹, Maria Teodora Wetscherek^{3,1}, Maria Dolores Sánchez-Valverde⁴, Lara Jaques-Pérez⁴, Lourdes Pérez-Rodríguez⁴, Kenji Takeda¹, José María Salinas⁵, Javier Alvarez-Valle¹, Joaquín Galant-Herrero⁴, and Antonio Pertusa⁶

¹ Microsoft Research, Cambridge, UK

² Medbravo, Alicante, Spain

³ Department of Radiology, University of Cambridge and Cambridge University Hospitals NHS Foundation Trust, Cambridge, UK

⁴ Department of Radiology, University Hospital Sant Joan d'Alacant, Spain

⁵ Department of Health Informatics, University Hospital Sant Joan d'Alacant, Spain

⁶ University Institute for Computing Research, University of Alicante, Spain

Abstract

BACKGROUND Radiology report generation (RRG) aims to create free-text radiology reports from clinical imaging. Grounded radiology report generation (GRRG) extends RRG by including the localisation of individual findings on the image. Currently, there are no manually annotated chest X-ray (CXR) datasets to train GRRG models.

METHODS In this work, we present a dataset called PadChest-GR (Grounded-Reporting) derived from PadChest aimed at training GRRG models for CXR images. First, a subset of studies was selected from PadChest using images with frontal projection, excluding paediatric patients and studies originally labelled as sub-optimal. Then, using GPT-4 in Microsoft Azure OpenAI Service, reports were processed to extract single-finding sentences, translate them from Spanish into English, link them to the existing PadChest finding and location labels, and classify finding progression. A team of 14 radiologists reviewed and manually annotated the findings in each image using bounding boxes, first discarding some studies with issues on the image quality, report, or findings list, and then annotating the boxes for each finding.

RESULTS We curate a public bi-lingual dataset of 4,555 CXR studies with grounded reports (3,099 abnormal and 1,456 normal), each containing complete lists of sentences describing individual present (positive) and absent (negative) findings in English and Spanish. In total, PadChest-GR contains 7,037 positive and 3,422 negative finding sentences. Every positive finding sentence is associated with up to two independent sets of bounding boxes labelled by different readers and has categorical labels for finding type, locations, and progression.

CONCLUSIONS To the best of our knowledge, PadChest-GR is the first manually curated dataset designed to train GRRG models for understanding and interpreting radiological images and generated text. By including detailed localization and comprehensive annotations of all clinically relevant findings, it provides a valuable resource for developing and evaluating GRRG models from CXR images. PadChest-GR can be downloaded under request from <https://bimcv.cipf.es/bimcv-projects/padchest-gr/>.

Introduction

In recent years, the use of artificial intelligence (AI) to improve medical image analysis has gained significant interest, with the potential to alleviate radiology workloads and enhance patient care [1, 2]. The modelling task of GRRG can be defined as predicting a list of sentences or phrases describing all individual findings in an image, with associated spatial annotations (e.g. bounding boxes) for localisable findings [3]. An example grounded report is shown in Fig. 1.

Because explainability is crucial in this domain [1], spatially grounding radiological findings is expected to help with verification of AI-generated draft reports [4]. Such grounding can also underpin new interactive capabilities of medical AI models [5], facilitating their interpretation by clinicians and even patients [2].

In the literature, there exist many CXR image datasets labelled for diagnosis and finding classification tasks [6, 7, 8, 9], or accompanied by textual radiology reports for automated draft report generation [10, 11, 12, 13]. Some datasets also include spatial annotations to localise labels (for finding, anatomy, or device; e.g. ‘pneumothorax’) [14, 15, 16, 17, 9, 12] or single finding phrases [18, 19], such as ‘*Left retrocardiac opacity*’. However, such datasets are not sufficient to construct full grounded reports, as they lack spatial annotations linked to complete sets of descriptive finding sentences [20].

Methods

SOURCE DATA

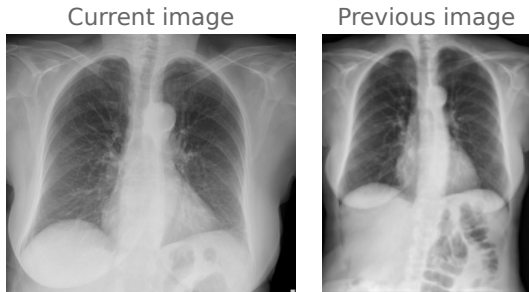
PadChest [6] is a large-scale CXR dataset which includes more than 160,000 images obtained from 67,000 patients that were interpreted and reported

by radiologists at the University Hospital Sant Joan d’Alacant (Spain) from 2009 to 2017. The reports were labeled with 174 different radiological findings, 19 differential diagnoses, and 104 anatomical locations organized as a hierarchical taxonomy and mapped onto standard Unified Medical Language System (UMLS) terminology [21]. The text reports publicly released with PadChest had been heavily processed to preserve anonymization, normalise capitalisation, punctuation, accents, stop-words, and affixes. For PadChest-GR, we retrieved the original reports for the entire PadChest cohort after anonymization and without further processing.

For inclusion in PadChest-GR, each radiographic study in PadChest was first linked to the patient’s most recent prior study based on the `StudyDate_DICOM` field. Studies from the same patient on the same date were excluded, as their order cannot be determined. We selected only frontal images (erect or supine, with projection ‘*PA*’, ‘*AP*’, or ‘*AP-horizontal*’) and excluded the few studies with more than one frontal image in either the current or prior study to avoid ambiguity. Paediatric patients (18 years old or younger) were also rejected, as well as studies acquired with a paediatric protocol. We also filtered out any studies that included the ‘*suboptimal*’, ‘*exclude*’, or ‘*unchanged*’ labels in PadChest, as they cannot be reliably annotated. Figure 2 summarises the pipeline for constructing PadChest-GR out of the 98,641 eligible PadChest studies.

STRATIFIED DATA SELECTION

We selected 4,000 abnormal studies (i.e. with at least one positive finding), chosen randomly via stratified sampling according to the distribution of finding categories in the eligible cohort. Note that approxi-

A

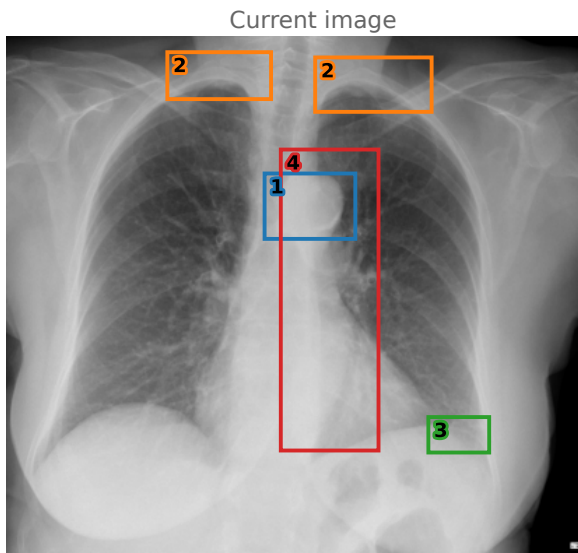
Labels (unordered)

- Finding category: aortic elongation
Locations: aortic → **4**
- Finding category: aortic atheromatosis
Locations: aortic → **1**
- Finding category: laminar atelectasis
Locations: basal, left → **3**
- Finding category: negative → **5**
- Finding category: apical pleural thickening
Locations: pleural → **2**

Report

Motivo de consulta: Preoperatorio.

Rx PA tórax:

Impresión diagnóstica: **Ateromatosis aórtica calcificada. Engrosamiento pleural biapical. Atelectasia laminar basal izquierda. Elongaación aórtica.** Sin otros hallazgos radiológicos significativos.**B**

Grounded Findings

- 1** [ES] Ateromatosis aórtica calcificada.
[EN] Calcified aortic atheromatosis.
Finding category: aortic atheromatosis
Locations: aortic
Progression label: None
- 2** [ES] Engrosamiento pleural biapical.
[EN] Bilateral apical pleural thickening.
Finding category: apical pleural thickening
Locations: pleural
Progression label: None
- 3** [ES] Atelectasia laminar basal izquierda.
[EN] Left basal laminar atelectasis.
Finding category: laminar atelectasis
Locations: left, basal
Progression label: None
- 4** [ES] Elongaación aórtica.
[EN] Aortic elongation.
Finding category: aortic elongation
Locations: aortic
Progression label: None
- 5** [ES] Sin otros hallazgos radiológicos significativos.
[EN] No other significant radiological findings.
Finding category: negative

Figure 1: Example of a grounded report from PadChest-GR. (Panel A) An original sample from PadChest [6], including a chest X-ray image, its free-text radiology report in Spanish, and categorical labels for radiological findings and anatomical locations (originally in English). We also show an image from the patient’s most recent prior study for comparison. (Panel B) The corresponding sample in PadChest-GR. The image is accompanied with a report in the form of a list of sentences individually describing at most one finding, in both English and Spanish. For findings that pertain to specific regions of the image, bounding boxes are provided to indicate the location. A finding can have more than one bounding box, for example in the case of bilateral observations. This comprehensive set of annotations for all finding sentences differs from existing datasets, which associate bounding boxes with only categorical labels or single sentences.

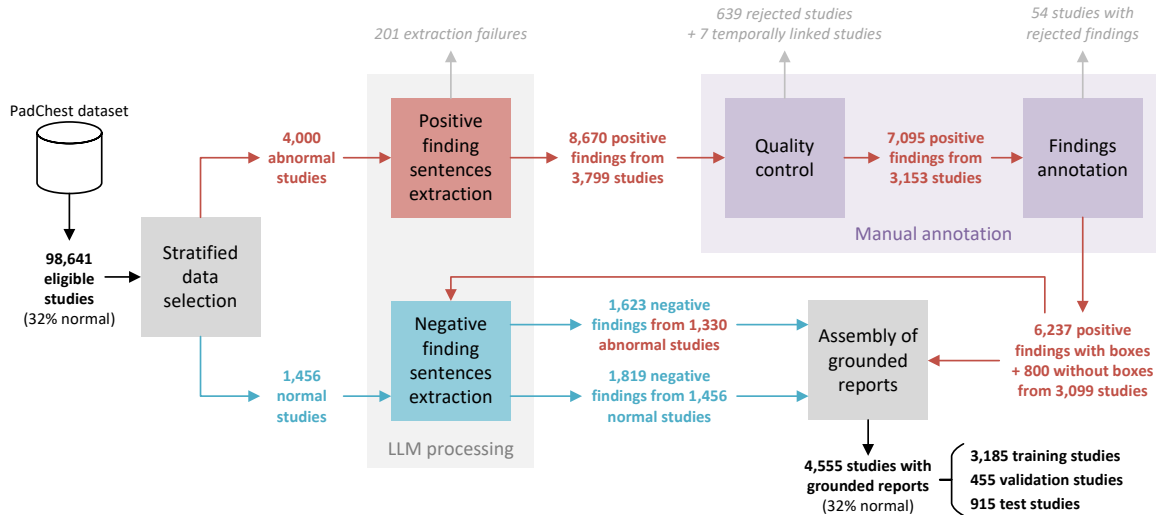


Figure 2: Illustration of the data curation pipeline. From the eligible PadChest studies, a set of studies with positive (i.e. abnormal) findings were selected with stratified sampling using a prespecified list of common and relevant finding categories. Normal studies (those with no positive findings) were also sampled to maintain the proportion of normal studies in the overall PadChest dataset (32.0%). From the findings section of each study, large language model (LLM) processing extracted and classified individual finding sentences (both positive and negative), and translated them to English. Positive findings were manually annotated by a team of radiologists to conduct both quality control and annotation of bounding boxes. Positive and negative findings sentences were assembled with these annotations in the original order for each study to produce a fully grounded report.

mately 25% of PadChest samples were originally labelled by radiologists, whereas the remaining cases were annotated automatically by a recurrent neural network with a per-label attention mechanism [22]. For PadChest-GR, we sampled only from the more reliable manually labelled subset.

Further, we highlight that the original PadChest finding ontology is too granular for stratification and analysis, as many detailed findings are rare in the dataset and could not be faithfully represented in the much smaller PadChest-GR dataset. Therefore, we first enumerated a non-exhaustive subset of finding types that were clinically relevant, broad enough for significant prevalence but not too vague, and visible

on a CXR. Finer-grained findings were subsumed into their parent super-categories (if selected) following the original PadChest hierarchy [6]; see full mapping in Table A.1. The final list of findings was further validated by a panel of radiologists. All categories that remained unmapped or had lower than 1% prevalence after this grouping were mapped to ‘Other’ (see Table B.1) and were simply not tracked for stratification, but the corresponding samples could still be included at random.

Finally, to preserve the composition of the original cohort, the dataset was complemented with normal studies—i.e. those with no positive findings according to the PadChest labels. After annotation and quality

control of the abnormal cases (as described later in ‘Manual annotation’ section), we randomly selected enough eligible normal studies to match their overall prevalence of 32.0%.

EXTRACTION OF FINDING SENTENCES

Sentences in routine free-text radiology reports frequently refer to multiple findings, and may also mention external information (e.g. patient history), communications between healthcare staff, clinical interpretation, follow-up recommendations, etc.—which cannot be objectively inferred from the radiographic study alone. On the other hand, grounded radiology reporting involves separately localising each observed finding [3]. Therefore, to enable annotation and model development for this task, existing radiology datasets must be processed to accurately extract sentences describing individual objective findings.

report in Spanish was processed to not only extract the single-finding sentences, but also translate the latter to English and link them to the existing PadChest labels.() See details and model instruction prompts in Appendix C. Positive and negative finding phrases were extracted in two separate stages.

For the positive findings, we leveraged PadChest’s existing finding and location labels, which were originally collected at the sentence level [6]. Labels for differential diagnoses that rely on additional clinical context, such as ‘*pneumonia*’, were ignored. The model was presented with the full original report and grouped sentence labels, and was asked to generate standalone sentences describing exclusively each of the given finding labels, along with English translations. Every extracted finding sentence was also matched to the relevant subset of provided location labels (see Appendix E). Further, the model classi-

fied the temporal progression of each finding, when applicable (see Fig. D.1).

Negative findings are statements referring to the absence of abnormal observations, such as ‘*No evidence of consolidation*’, ‘*Heart size is normal*’, or ‘*No significant findings*’. In PadChest, negative findings were not labelled for the specific negated findings or their locations [6]. We therefore relied on the LLM to identify negative finding sentences and split them if necessary. Following [3], we tasked the LLM with extracting sentences describing individual observations, with two additional requirements: (1) translation to English, and (2) classification of sentences as either positive or negative findings. This enables us to extract only the negative findings.

MANUAL ANNOTATION

The selected studies were annotated by nine senior and five junior radiologists from the University Hospital Sant Joan d’Alacant, Spain, using the HIPAA-compliant Centaur Labs labelling service (<https://www.centaurlabs.com>). The annotation was performed in two stages: study-level quality control followed by box annotations for each extracted positive finding. For both stages, every study or finding was analysed independently by two professionals. The current frontal image was always displayed beside the linked prior image when available, so that findings reported with temporal progression could be accurately identified.

First, for each radiological study, annotators were presented with the original report in Spanish and the list of all extracted positive finding sentences in both Spanish and English (see Fig. 3A). The study was assessed for any major issues with the image quality, report quality, selection of the prior image, or list

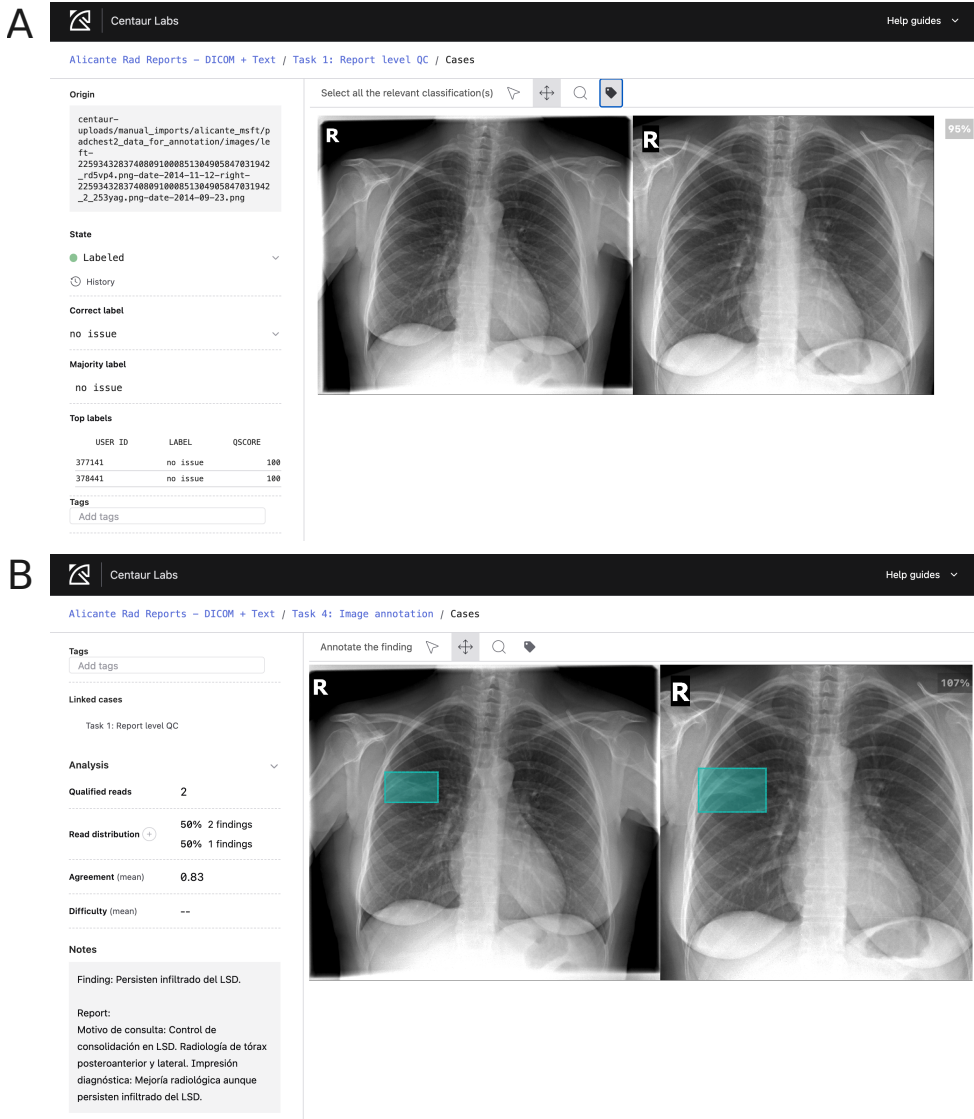


Figure 3: Screenshots of the interface for both manual annotation stages. (Panel A) Example of study-level quality control, containing infiltrates in the current (left) and prior (right) images. In this stage, the radiologists select the category (for this study, ‘no issue’) according to the quality of the image, the report, and the extracted findings. (Panel B) Example of bounding box annotation for an individual finding (‘Infiltrates in the right upper lobe persist’) from the same study. All annotations were performed using the Centaur Labs platform.

of findings, as well as for the presence of unfiltered protected health information or paediatric patients. Radiologists also discarded those studies for which the lateral projection was necessary to assess a finding. If any such issue was flagged, the study was removed from further annotation, and agreement between both radiologists was required to accept each case. The 989 cases with no consensus were reevaluated by a group of three senior radiologists, requiring approval by at least two of them. We additionally discarded 7 studies linked to rejected prior studies.

In the second stage, those images passing the quality control stage were annotated. Each positive finding sentence was reviewed individually by two radiologists. If the finding was localisable, each annotator drew one or more tight bounding boxes covering the area(s) where it was visible in the image, as shown in Fig. 3B. In particular, for diffuse findings whose bounding box(es) would cover more than half of the image, annotators were instructed not to draw any boxes.

ANNOTATION POST-PROCESSING AND ARBITRATION

We filtered out individual boxes with areas smaller than 0.1% of the respective image, likely corresponding to spurious clicks in the annotation interface. Then, for each finding, we arbitrated which of the two annotations (i.e. sets of boxes) should be treated as official. This was done by applying a sequence of binary criteria to both annotations until a unique choice could be made. In order of priority, we preferred the annotation that: (1) has any boxes; (2) has at least 80% of its area contained in the other, therefore assumed to be more precise; (3) was created by a senior radiologist; (4) has more boxes; (5) has smaller

overall area. All remaining 436 cases (7.0%) were decided at random. The unselected extra annotations are also released as part of the dataset, for researchers interested in studying inter-observer variability.

ASSEMBLY OF GROUNDED REPORTS

Each finding sentence was extracted along with a source span from the original report. The positions of these excerpts in the text were then used to merge and sort the lists of positive and negative findings in the same order as originally reported.

In order to standardise the data for training machine learning models, we partitioned 70% of studies for training, 10% for validation, and the remaining 20% for testing. Splits were determined at random, stratified by the same finding categories as for data selection, and ensuring all studies of each patient were kept within a single partition. This process was also applied to the remaining eligible studies outside of PadChest-GR, resulting in a stratified split for the entire PadChest dataset.

Results

DATASET COMPOSITION

The resulting PadChest-GR dataset is composed of 4,555 studies, of which 1,456 (32%) are normal and 3,099 (68%) abnormal. The median age is 69 years, and samples have an equal representation of men and women, with a balanced distribution between the two groups (see Fig. 4A). The studies included in PadChest-GR were all acquired in 2014–2017, as this was the time range selected for manual annotation in PadChest [6]. Prior images are available for 31.7% of all studies. As expected, Fig. 4B shows this proportion is higher among abnormal studies (34.4%)

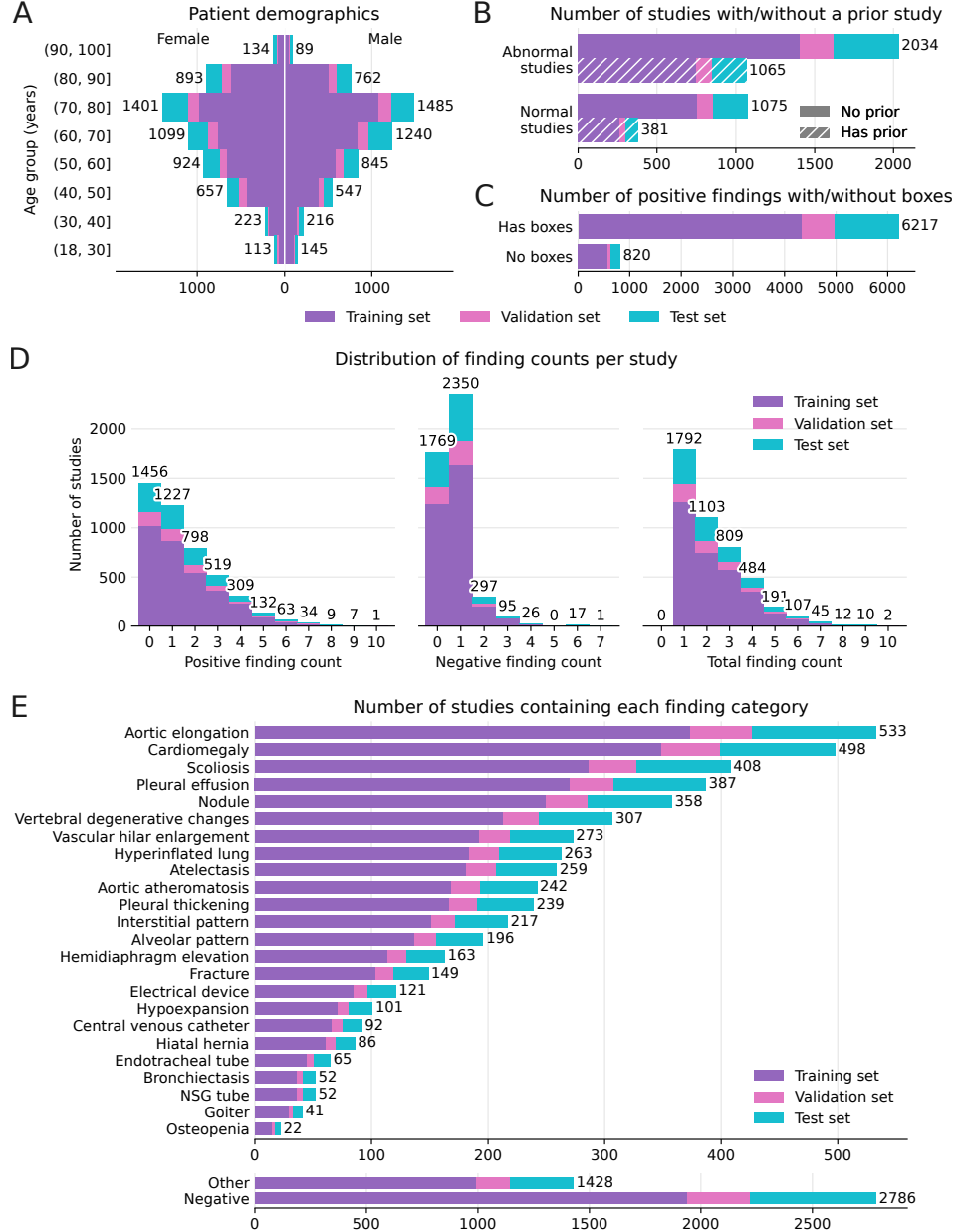


Figure 4: Descriptive statistics for the studies included in the PadChest-GR dataset. (Panel A) Joint distribution of patient sex and age. (Panel B) Availability of a prior study for abnormal and normal studies. (Panel C) Availability of manual box annotations per positive finding. (Panel D) Histograms of number of individual finding sentences (positive, negative, and total) per study. (Panel E) Distribution of the 24 finding categories, as well as studies including ‘Other’ and negative findings. Note how all distributions of demographics, availability of prior studies, and finding counts are well represented across training, validation, and test partitions.

than normal ones (26.2%), since patients with positive findings are more likely to require follow-up scans for monitoring.

PadChest-GR includes 7,037 positive findings and 3,422 negative findings in total. On average, the grounded report for each abnormal study contains 2.27 positive and 0.52 negative findings, whereas normal studies have 1.25 negative findings. Detailed distributions are shown in Fig. 4D. We observe a long tail of positive finding counts, with 246 studies (5.4%) containing five or more. An overwhelming majority (84.4%) of all 2,786 reports that include any negative findings has a single one, typically equivalent to “no (other) significant findings”.

Figure 4E shows the distribution of the main 24 finding categories, with a balanced representation across all partitions.

Progression status (see Fig. D.1) was available for 306 finding sentences (11.4% of all positive findings) in studies with linked prior studies and 323 (7.4%) in studies without. Combined, the evolution of these findings was as follows: 386 stable (61.3%), 108 improving (17.2%), 71 worsening (11.3%), 56 new (8.9%), and 8 resolved (1.3%). The five most common finding categories with progression status were pleural effusion, nodule, alveolar pattern, interstitial pattern, and atelectasis.

Location labels with anatomical regions were available for 64.3% of the finding sentences. In addition to the selected list of finding categories used for stratification, radiologists also labelled a total of 1,956 finding sentences that were not included in the primary stratification criteria. These additional findings were labelled with bounding boxes because they were deemed clinically relevant or radiologically visible. The complete list of these additional entities, along with their respective counts of images and bounding

boxes, is provided in Table B.1, being the 4 most frequent entities chronic changes, infiltrates, fibrotic band and increased density.

BOX ANNOTATIONS

Box annotation statistics are visualised in Fig. 5. We observe that certain hardware categories—including electrical device (e.g. pacemaker), nasogastric tube, and central venous catheter—tend to have relatively large boxes. This is because the rectangular annotations cover the full horizontal and vertical extent of the long tubes and pacemaker wires, as evidenced by the spatial heatmaps in Fig. 5B.

It is also worth noting the variability in how radiologists annotated some finding categories, e.g. nodules and interstitial/alveolar patterns. At times, the latter were annotated with multiple small boxes precisely localising each instance in the image, and, in other cases, with larger boxes encompassing the whole affected areas. Up to 81.9% of finding sentences have associated anatomical location labels (Appendix E).

Lastly, note that 11.7% of the total 7,037 positive findings were not localised with boxes, as indicated in Fig. 4C. Consistently with the annotation instructions, this happened particularly often for diffuse, chronic, or global finding categories, such as osteopenia, bronchiectasis, hyperexpansion, and hypoinflation. Extra box annotations are available for 5,242 findings, with a median intersection-over-union of 0.530 compared to the official boxes.

Discussion

In this work, we present PadChest-GR, a first-in-class dataset designed to train and evaluate grounded re-

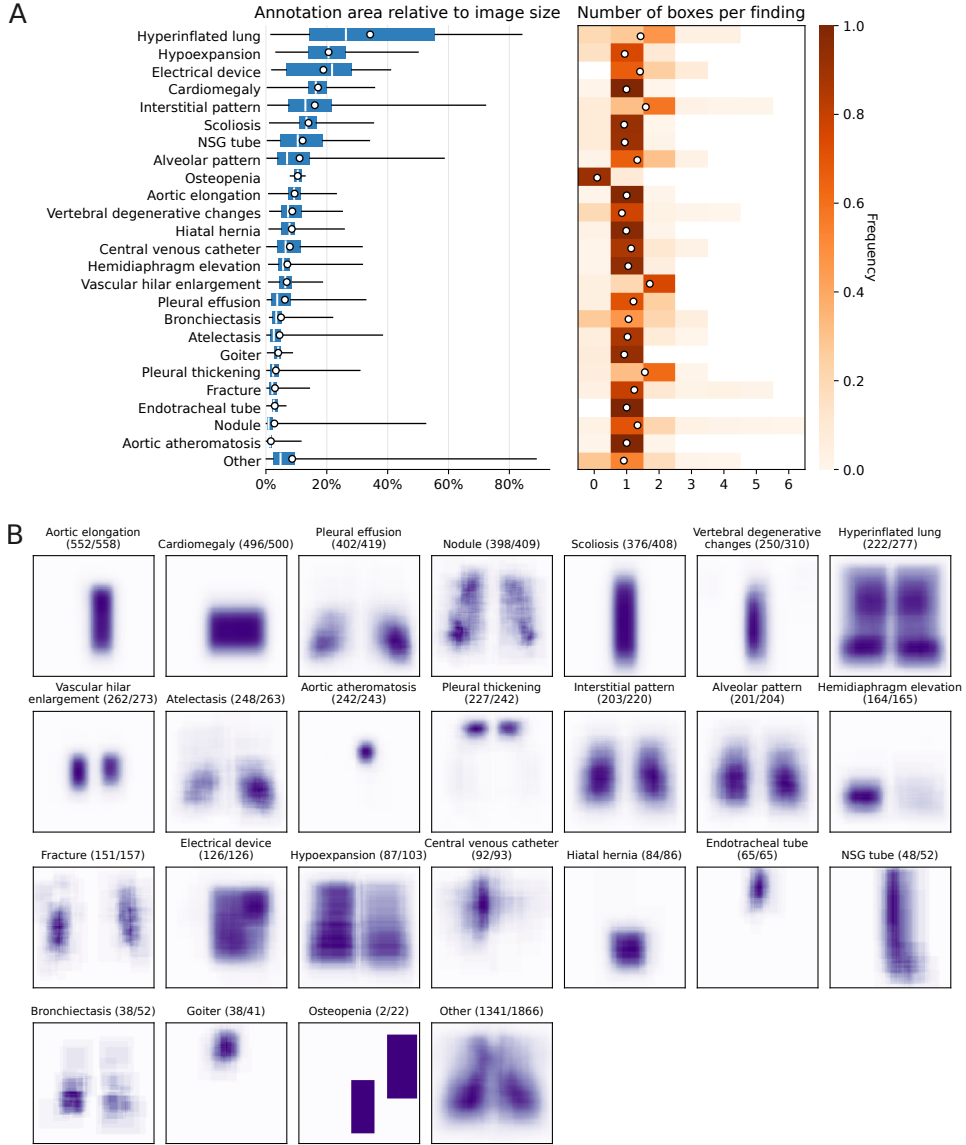


Figure 5: Descriptive statistics for the official box annotations included in the PadChest-GR dataset, stratified by finding category. (Panel A) Distributions of total area (box plots, left) and number of boxes (histograms, right) per annotation, sorted by mean area. Box plots indicate minimum/maximum, quartiles, median (vertical line), and mean (circle). Histograms additionally show the mean (circle). (Panel B) Heatmaps illustrating how often each pixel location was contained in a set of boxes for a finding in the given category. The numbers in parentheses indicate the counts of individual findings annotated with boxes and the total. Note that 224 studies contain two or more finding sentences in the same category. The scale of each heatmap is normalised independently for visualisation purposes.

port generation models from CXR images. A key differentiator of PadChest-GR is the inclusion of comprehensive sentence-level bounding box annotations for all clinically relevant findings in each image, as judged by expert radiologists. Samples with missing findings were filtered out during quality control, ensuring completeness of the grounded reports.

PadChest-GR offers several advantages that enhance the dataset’s utility. First, it provides bilingual (Spanish and English) sentence-level findings alongside fine-grained standardised terminology, enhancing accessibility and utility across different linguistic contexts. Also, most bounding boxes are accompanied by location labels, providing multimodal spatial information for abnormalities. In addition, the dataset includes progression status and prior X-rays for a subset of studies, enabling research into disease evolution. Further, its comprehensive annotations with sentence-level structure support direct evaluation of logical, grounding, and spatial entailment using metrics such as RadFact [3].

Inter-observer variability and subjectivity pose challenges for annotation, modelling, and evaluation—especially for borderline or diffuse findings. To address this, PadChest-GR includes annotations from two radiologists per finding, offering alternative perspectives and highlighting uncertainties.

LIMITATIONS

We acknowledge some PadChest-GR limitations, most of them derived from the use of the original PadChest[6] data. First, although this dataset represents a large, retrospective cohort, it originates from a single hospital in Spain, likely containing biases related to regional healthcare practices, and does not

fully represent diverse populations.

Regarding image quality, all studies were acquired between 2014 and 2017, with many digitized from radiological films rather than captured digitally, resulting in lower image quality compared to contemporary standards. The images are in PNG format with a reduced grayscale range compared to DICOM, affecting the visibility of subtle findings, such as interstitial lung disease patterns or small pneumothoraces. Additionally, during annotation, radiologists were unable to adjust window width and level or apply image filters, affecting their assessment of certain areas, such as the pulmonary interstitium, retrocardiac regions, and the visualization of tubes and catheters. Moreover, the cohort includes many bedridden and ICU patients, whose radiographs are of lower quality due to immobility and suboptimal positioning. Nonetheless, non-optimal image quality reflects realistic conditions for training and testing robust models.

Regarding projection limitations, the dataset predominantly contains postero-anterior (PA) images without corresponding lateral views. Certain findings, such as vertebral fractures, hyperkyphosis, and pulmonary hyperinflation, are better assessed on lateral projections. The absence of lateral views meant that some findings in the reports could not be corroborated or annotated on the available images and were discarded, limiting the representation of pathologies that are projection-dependent.

Although LLMs have demonstrated impressive capabilities in de-identification [23], translation [24], and error detection in radiology reports [25], they are not without flaws. In our data processing, GPT-4 occasionally produced truncated sentences during automated extraction from reports. However, labels from the original PadChest dataset ensured that associ-

ated findings were annotated on the images. We also noted some literal translations such as ‘condensation’ instead of ‘consolidation’, though they are consistent across studies.

It is also worth noting that the time interval with prior radiographs available in PadChest was not always optimal for disease comparison, especially in cases of acute pathology. This inconsistency could limit the assessment of disease progression or the evaluation of temporal changes, which are important aspects in longitudinal studies.

CONCLUSIONS AND FUTURE WORK

By providing comprehensive annotations of all clinically relevant findings along with their localisations, we hope that PadChest-GR will foster new avenues in medical imaging research and support the development of more robust and interpretable models in radiology.

To address the limitations mentioned, future efforts could focus on enhancing diversity by incorporating data from multiple institutions to improve generalisability. Additionally, including higher-resolution images in the standard DICOM format would facilitate more detailed visualization and analysis. Finally, expanding the dataset to include lateral views and other relevant imaging modalities would allow for a more comprehensive findings assessment.

Notes

We thank the radiologists team from from Sant Joan d’Alacant Hospital—led by Joaquín Galant Herrero and composed by María Dolores Sánchez Valverde, Lara Jaques Pérez, Lourdes Pérez Rodríguez, Marife Lorente Fernández, Jorge Calbo Maiques, María Culiáñez Casas, Laila Santirso Abuelbar, Diego Mauricio Angulo Henao, Vicente Pedro Davó Quiñonero, María Begerano Fayos, Jorge Caballero Serra, Rocío Belda

Márquez, and Carla Fuster Redondo—for their contributions with data annotation. We further thank Fabian Falck, Fernando Pérez-García, and Harshita Sharma for their valuable feedback on the manuscript, Anton Schwaighofer for the software infrastructure support, Max Ilse for early contributions to the methodology, and Hannah Richardson for help navigating data compliance.

This work was led by the PadChest team and supported by project UA-MICROSOFT01 from the University of Alicante, funded by Microsoft Corporation and coordinated by Antonio Pertusa.

CRedit author statement: D.C.C.: Conceptualization, Data curation, Formal analysis, Methodology, Project administration, Software, Visualization, Writing – original draft, Writing – review & editing. A.B.: Conceptualization, Formal analysis, Methodology, Software, Visualization, Writing – original draft, Writing – review & editing. S.B.: Data curation, Methodology, Software, Visualization, Writing – review & editing. S.L.H.: Conceptualization, Data curation, Methodology, Software, Writing – review & editing. K.B.: Data curation, Methodology, Software, Writing – review & editing. M.T.W.: Data curation, Methodology, Writing – review & editing. M.D.S.V., L.J.P., and L.P.R.: Investigation (data annotation). K.T.: Conceptualization, Funding acquisition, Project administration, Writing – original draft, Writing – review & editing. J.M.S.: Conceptualization, Project administration, Resources. J.A.V.: Conceptualization, Funding acquisition, Project administration, Resources, Writing – review & editing. J.G.H.: Conceptualization, Investigation (data annotation), Methodology, Project administration, Writing – review & editing. A.P.: Conceptualization, Funding acquisition, Project administration, Supervision, Writing – original draft, Writing – review & editing.

References

- [1] Pranav Rajpurkar and Matthew P Lungren. The current and future state of ai interpretation of medical images. *N Engl J Med*, 388(21):1981–1990, 2023.
- [2] Nur Yildirim, Hannah Richardson, Maria Teodora Wetscherek, Junaid Bajwa, Joseph Jacob, Mark Ames Pinnock, Stephen Harris, Daniel C. Castro, Shruthi Bannur,

Stephanie Hyland, Pratik Ghosh, Mercy Ranjit, Kenza Bouzid, Anton Schwaighofer, Fernando Pérez-García, Harshita Sharma, Ozan Oktay, Matthew Lungren, Javier Alvarez-Valle, Aditya Nori, and Anja Thieme. Multimodal healthcare AI: Identifying and designing clinically relevant vision-language applications for radiology. In *Proceedings of the 2024 CHI Conference on Human Factors in Computing Systems*, page 444, 2024.

[3] Shruthi Bannur, Kenza Bouzid, Daniel C. Castro, Anton Schwaighofer, Sam Bond-Taylor, Maximilian Ilse, Fernando Pérez-García, Valentina Salvatelli, Harshita Sharma, Felix Meissen, Mercy Ranjit, Shaury Srivastav, Julia Gong, Fabian Falck, Ozan Oktay, Anja Thieme, Matthew P. Lungren, Maria Teodora Wetscherek, Javier Alvarez-Valle, and Stephanie L. Hyland. MAIRA-2: Grounded radiology report generation, 2024.

[4] Michael H Bernstein, Michael K Atalay, Elizabeth H Dibble, Aaron WP Maxwell, Adib R Karam, Saurabh Agarwal, Robert C Ward, Terrence T Healey, and Grayson L Baird. Can incorrect artificial intelligence (AI) results impact radiologists, and if so, what can we do about it? A multi-reader pilot study of lung cancer detection with chest radiography. *European Radiology*, 33(11):8263–8269, 2023.

[5] Michael Moor, Oishi Banerjee, Zahra Shakeri Hossein Abad, Harlan M. Krumholz, Jure Leskovec, Eric J. Topol, and Pranav Rajpurkar. Foundation models for generalist medical artificial intelligence. *Nature*, 616(7956):259–265, April 2023.

[6] Aurelia Bustos, Antonio Pertusa, Jose-Maria Salinas, and Maria De La Iglesia-Vayá. Pad-Chest: A large chest x-ray image dataset with multi-label annotated reports. *Medical Image Analysis*, 66:101797, 2020.

[7] Jeremy Irvin, Pranav Rajpurkar, Michael Ko, Yifan Yu, Silviana Ciurea-Ilcus, Chris Chute, Henrik Marklund, Behzad Haghgoo, Robyn L. Ball, Katie Shpanskaya, Jayne Seekins, David A. Mong, Safwan S. Halabi, Jesse K. Sandberg, Ricky Jones, David B. Larson, Curtis P. Langlotz, Bhavik N. Patel, Matthew P. Lungren, and Andrew Y. Ng. CheXpert: A large chest radiograph dataset with uncertainty labels and expert comparison. In *Proceedings of the AAAI Conference on Artificial Intelligence (AAAI 2019)*, volume 33, pages 590–597. AAAI Press, July 2019.

[8] Jean-Benoit Delbrouck, Pierre Chambon, Zhi-hong Chen, Maya Varma, Andrew Johnston, Louis Blankemeier, Dave Van Veen, Tan Bui, Steven Truong, and Curtis Langlotz. RadGraph-XL: A large-scale expert-annotated dataset for entity and relation extraction from radiology reports. In *Findings of the Association for Computational Linguistics ACL 2024*, pages 12902–12915, August 2024.

[9] Xiaosong Wang, Yifan Peng, Le Lu, Zhiyong Lu, Mohammadhadhi Bagheri, and Ronald M. Summers. ChestX-ray8: Hospital-scale chest X-ray database and benchmarks on weakly-supervised classification and localization of common thorax diseases. In *Proceedings of the IEEE Conference on Computer Vision and Pattern Recognition (CVPR)*, pages 2097–2106. IEEE, 2017.

[10] Alistair E. W. Johnson, Tom J. Pollard, Seth J. Berkowitz, Nathaniel R. Greenbaum, Matthew P. Lungren, Chih-ying Deng, Roger G. Mark, and Steven Horng. MIMIC-CXR, a de-identified publicly available database of chest radiographs with free-text reports. *Scientific Data*, 6(1):317, December 2019.

[11] Dina Demner-Fushman, Marc D Kohli, Marc B Rosenman, Sonya E Shooshan, Laritza Rodriguez, Sameer Antani, George R Thoma, and Clement J McDonald. Preparing a collection of radiology examinations for distribution and retrieval. *Journal of the American Medical Informatics Association*, 23(2):304–310, 2016.

[12] Sijing Feng, Damian Azzollini, Ji Soo Kim, Cheng-Kai Jin, Simon P. Gordon, Jason Yeoh,

Eve Kim, Mina Han, Andrew Lee, Aakash Patel, Joy Wu, Martin Urschler, Amy Fong, Cameron Simmers, Gregory P. Tarr, Stuart Barnard, and Ben Wilson. Curation of the candid-ptx dataset with free-text reports. *Radiology: Artificial Intelligence*, 3(6):e210136, 2021.

[13] Pierre Chambon, Jean-Benoit Delbrouck, Thomas Sounack, Shih-Cheng Huang, Zhi-hong Chen, Maya Varma, Steven QH Truong, Chu The Chuong, and Curtis P. Langlotz. CheXpert Plus: Augmenting a large chest X-ray dataset with text radiology reports, patient demographics and additional image formats, 2024.

[14] Joy Wu, Yaniv Gur, Alexandros Karargyris, Ali Bin Syed, Orest Boyko, Mehdi Moradi, and Tanveer Syeda-Mahmood. Automatic bounding box annotation of chest x-ray data for localization of abnormalities. In *2020 IEEE 17th International Symposium on Biomedical Imaging (ISBI)*, pages 799–803, 2020.

[15] Joy T Wu, Nkechinyere Agu, Ismini Lourentzou, Ismini Lourentzou, Arjun Sharma, Joseph Alexander Paguio, Jasper Seth Yao, Edward C Dee, William Mitchell, Satyananda Kashyap, Andrea Giovannini, Leo Anthony Celi, and Mehdi Moradi. Chest ImaGenome dataset for clinical reasoning, 2021.

[16] Ricardo Bigolin Lanfredi, Joyce D. Schroeder, and T. Tasdizen. Localization supervision of chest x-ray classifiers using label-specific eye-tracking annotation. *Frontiers in radiology*, 3, 2022.

[17] Ha Q Nguyen, Khanh Lam, Linh T Le, Hieu H Pham, Dat Q Tran, Dung B Nguyen, Dung D Le, Chi M Pham, Hang TT Tong, Diep H Dinh, et al. VinDr-CXR: An open dataset of chest X-rays with radiologist’s annotations. *Scientific Data*, 9(1):429, 2022.

[18] Benedikt Boecking, Naoto Usuyama, Shruthi Bannur, Daniel Coelho de Castro, Anton Schwaighofer, Stephanie Hyland, Maria Teodora Wetscherek, Tristan Naumann, Aditya Nori, Javier Alvarez Valle, Hoifung Poon, and Ozan Oktay. MS-CXR: Making the most of text semantics to improve biomedical vision-language processing (version 0.1), 2022.

[19] Shruthi Bannur, Stephanie Hyland, Qianchu Liu, Fernando Pérez-García, Max Ilse, Daniel Coelho de Castro, Benedikt Boecking, Harshita Sharma, Kenza Bouzid, Anton Schwaighofer, Maria Teodora Wetscherek, Hannah Richardson, Tristan Naumann, Javier Alvarez Valle, and Ozan Oktay. MS-CXR-T: Learning to exploit temporal structure for biomedical vision-language processing (version 1.0.0), 2023.

[20] Zhiyong Lu, Yifan Peng, Trevor Cohen, Marzyeh Ghassemi, Chunhua Weng, and Shubo Tian. Large language models in biomedicine and health: current research landscape and future directions. *Journal of the American Medical Informatics Association*, 31(9):1801–1811, 08 2024.

[21] Olivier Bodenreider. The Unified Medical Language System (umls): integrating biomedical terminology. *Nucleic Acids Research*, 32(suppl1):D267–D270, January 2004.

[22] James Mullenbach, Sarah Wiegreffe, Jon Duke, Jimeng Sun, and Jacob Eisenstein. Explainable prediction of medical codes from clinical text. In *Proceedings of the 2018 Conference of the North American Chapter of the Association for Computational Linguistics: Human Language Technologies, Volume 1 (Long Papers)*, volume 1, pages 1101–1111, 2018.

[23] Yuxin Xiao, Shulammite Lim, Tom Joseph Pollard, and Marzyeh Ghassemi. In the name of fairness: Assessing the bias in clinical record de-identification. In *Proceedings of the 2023 ACM Conference on Fairness, Accountability, and Transparency*, pages 123–137, 2023.

[24] Praneet Khanna, Gagandeep Dhillon, Venkata Buddhavarapu, Ram Verma, Rahul Kashyap, and Harpreet Grewal. Artificial intelligence

in multilingual interpretation and radiology assessment for clinical language evaluation (AI-MIRACLE). *Journal of Personalized Medicine*, 14(9):923, 2024.

- [25] Roman Johannes Gertz, Thomas Dratsch, Alexander Christian Bunck, Simon Lennartz, Andra-Iza Iuga, Martin Gunnar Hellmich, Thorsten Persigehl, Lenhard Pennig, Carsten Herbert Gietzen, Philipp Fervers, David Maintz, Robert Hahnfeldt, Jonathan Kottlors, and Linda Moy. Potential of GPT-4 for detecting errors in radiology reports: Implications for reporting accuracy. *Radiology*, 311(1):e232714, 2024.
- [26] OpenAI. Gpt-4 technical report, 2024.

A Finding label mapping for stratification

Table A.1: Finding group labels used for stratification. Grouping of finding labels was done manually in conjunction with a consultant radiologist.

Group label	Finding label	Image count	Boxes count
Negative	N/A	1456	0
Aortic elongation	aortic elongation	464	465
	aortic button enlargement	38	33
	descendent aortic elongation	27	27
	supra aortic elongation	27	31
	ascendent aortic elongation	2	2
Cardiomegaly	cardiomegaly	498	495
	pericardial effusion	2	2
Nodule	pseudonodule	103	132
	calcified granuloma	100	139
	nodule	89	107
	nipple shadow	68	100
	pulmonary mass	24	24
	granuloma	20	28
	multiple nodules	13	33
	end on vessel	5	5
	mass	4	4
	soft tissue mass	4	4
	miliary opacities	2	4
	pleural mass	1	1
Pleural effusion	pleural effusion	208	264
	costophrenic angle blunting	191	226
	minor fissure thickening	16	14
	loculated pleural effusion	4	4
	loculated fissural effusion	3	3
	fissure thickening	2	2
	major fissure thickening	2	2
Scoliosis	scoliosis	408	377
Vertebral degenerative changes	vertebral degenerative changes	269	263
	vertebral anterior compression	41	2
	vertebral compression	3	1
Hyperinflated lung	air trapping	225	316
	flattened diaphragm	32	52
	hyperinflated lung	22	32
Vascular hilar enlargement	vascular hilar enlargement	193	325
	hilar congestion	78	139
	pulmonary artery enlargement	2	4
Atelectasis	laminar atelectasis	154	164
	atelectasis	87	84
	lobar atelectasis	11	12
	atelectasis basal	6	5
	segmental atelectasis	4	4
	total atelectasis	1	1

Table A.1: Group labels used for stratification (cont.)

Group label	Finding label	Image count	Boxes count
Aortic atheromatosis	aortic atheromatosis	243	243
Pleural thickening	apical pleural thickening	205	333
	pleural thickening	20	25
	calcified pleural thickening	11	12
	calcified pleural plaques	6	8
Interstitial pattern	interstitial pattern	195	311
	ground glass pattern	11	16
	reticular interstitial pattern	10	16
	reticulonodular interstitial pattern	4	7
Alveolar pattern	alveolar pattern	146	211
	consolidation	42	43
	cavitation	14	15
	air bronchogram	2	2
	abscess	1	1
Electrical device	pacemaker	104	147
	dual chamber device	35	53
	single chamber device	19	26
	DAI (implantable cardioverter-defibrillator)	14	20
	electrical device	4	4
Hemidiaphragm elevation	diaphragmatic eventration	84	92
	hemidiaphragm elevation	81	81
Fracture	callus rib fracture	108	144
	rib fracture	22	25
	humeral fracture	13	13
	clavicle fracture	10	11
	vertebral fracture	3	0
	fracture	1	1
Hypoexpansion	volume loss	75	68
	hypoexpansion	28	29
Central venous catheter	central venous catheter via jugular vein	46	47
	central venous catheter via subclavian vein	17	24
	central venous catheter	15	19
	reservoir central venous catheter	15	16
Hiatal hernia	hiatal hernia	86	85
Endotracheal tube	endotracheal tube	39	39
	tracheostomy tube	26	26
NSG tube	NSG tube	52	49
Bronchiectasis	bronchiectasis	52	55
Goiter	goiter	41	38
Osteopenia	osteopenia	13	1
	osteoporosis	9	1

B Other finding types not used for stratification

Table B.1: Other finding types not used for stratification

Finding label	Image count	Boxes count
chronic changes	493	223
infiltrates	154	171
fibrotic band	153	177
increased density	112	120
kyphosis	103	8
sternotomy	76	79
suture material	74	73
hilar enlargement	69	115
metal	55	60
gynecomastia	53	92
calcified densities	41	49
mammary prosthesis	41	73
osteosynthesis material	41	41
bronchovascular markings	33	40
sclerotic bone lesion	28	30
tracheal shift	27	27
bullas	25	35
azygos lobe	24	24
mastectomy	23	24
superior mediastinal enlargement	23	23
mediastinic lipomatosis	21	21
mediastinal enlargement	17	17
vascular redistribution	17	18
axial hyperostosis	15	10
surgery breast	15	17
non axial articular degenerative changes	14	19
surgery	14	12
thoracic cage deformation	13	15
artificial heart valve	10	9
costochondral junction hypertrophy	10	11
pneumothorax	10	8
surgery neck	10	10
calcified adenopathy	9	11
adenopathy	8	6
mediastinal mass	8	8
surgery lung	8	5
chest drain tube	7	7
obesity	7	1
artificial mitral heart valve	6	6
central vascular redistribution	6	7
pectum excavatum	6	0
heart valve calcified	5	5
humeral prosthesis	5	5
air fluid level	4	4
cervical rib	4	6
kerley lines	4	7
pneumoperitoneo	4	6
abnormal foreign body	3	3
artificial aortic heart valve	3	3
catheter	3	3

Table B.1: Other finding types not used for stratification (cont.)

Finding label	Image count	Boxes count
lytic bone lesion	3	3
prosthesis	3	3
sternoclavicular junction hypertrophy	3	3
subacromial space narrowing	3	4
subcutaneous emphysema	3	3
surgery heart	3	3
aortic aneurysm	2	2
aortic endoprosthesis	2	2
azygoesophageal recess shift	2	2
blastic bone lesion	2	4
calcified fibroadenoma	2	2
cyst	2	2
hydropneumothorax	2	2
lung vascular paucity	2	2
surgery humeral	2	2
Chilaидти sign	1	1
endoprosthesis	1	1
gastrostomy tube	1	1
mediastinal shift	1	1
pectum carinatum	1	0
ventriculoperitoneal drain tube	1	1

C Language model prompting details

We employed OpenAI GPT-4 [26] v0613 via a private instance of the Microsoft Azure OpenAI service. The processing was done in a structured way to extract single-finding sentences, translate them to English, link them to the existing PadChest labels, and copy each source sentence to allow reconstructing full grounded reports in the right order. The expected output formats were specified by including the respective JSON schema in the model prompt, and outputs were validated to ensure consistency of the extracted metadata, using the Pydantic Python library. GPT-4 worked more reliably than GPT-3.5 Turbo for these highly structured tasks and it was capable of processing all sentences simultaneously and without in-context examples (for positive findings extraction). For extracting negative findings, 11 in-context examples were provided.

Code Snippet C.1: GPT-4 prompt for extracting positive finding phrases.

```
# System
You are an AI radiology assistant who is fluent in English and Spanish. You are helping process radiology reports
from chest X-rays.

Note that, in Spanish, lung lobes are referred by abbreviations, for example: "LSD" for "lóbulo superior derecho"
(right upper lobe).

You will receive a report in Spanish prefixed by "REPORT:". For different sentences in the report, you will receive
a list of finding types prefixed by "SENTENCE FINDINGS:", and possibly a list of location labels prefixed by
"SENTENCE LOCATIONS:", if available.

Instructions:
- You must process the sentence labels in the same order as given in the query.
- For each group of labels, extract verbatim the sentence from the report that describes them.
- For each finding label, provide a standalone phrase describing specifically the requested finding. It should be as
close as possible to the full original sentence and not mention any other findings. Include as much context from the
report as necessary for the phrase to make sense on its own.
- All finding labels must be processed, even if they are redundant.
- For each extracted sentence and generated phrase, also include an accurate translation in English.
- If finding labels are provided, identify which of these correspond to each finding. All of the provided location
labels must be exactly matched to at least one finding in the same sentence, even if they are redundant.
- If a finding is reported with a comparison to a prior exam, classify the progression of the condition as "new",
"worsening", "stable", "improving", or "resolved". If there is no comparison, set progression to "N/A".

The output should be formatted as a JSON instance that conforms to the JSON schema below.

As an example, for the schema {"properties": {"foo": {"title": "Foo", "description": "a list of strings", "type": "array", "items": {"type": "string"}}, "required": ["foo"]}}
the object {"foo": ["bar", "baz"]} is a well-formatted instance of the schema. The object {"properties": {"foo": ["bar", "baz"]}} is not well-formatted.

Here is the output schema:
"""
{json_schema}
"""

# User
REPORT: {report_es}
-----
SENTENCE FINDINGS: {sentence_labels[0].finding}
SENTENCE LOCATIONS: {sentence_labels[0].locations}
-----
```

```

SENTENCE FINDINGS: {sentence_labels[1].findings}
SENTENCE LOCATIONS: {sentence_labels[1].locations}
-----
...

```

Code Snippet C.2: GPT-4 instruction for extracting negative finding phrases.

You are an AI radiology assistant. You are helping process reports from chest X-rays.

Please extract phrases from the radiology report which refer to objects, findings, or anatomies visible in a chest X-ray, or the absence of such.

Rules:

- If a sentence describes multiple findings, split them up into separate sentences.
- Exclude clinical speculation or interpretation (e.g. "... highly suggestive of pneumonia").
- Exclude recommendations (e.g. "Recommend a CT").
- Exclude comments on the technical quality of the X-ray (e.g. "there are low lung volumes").
- Include mentions of change (e.g. "Pleural effusion has increased") because change is visible when we compare two X-rays.
- If consecutive sentences are closely linked such that one sentence can't be understood without the other one, process them together.
- Mark whether the phrase refers to something normal ("non_finding"), abnormal ("finding"), or ambiguous.

The objective is to extract phrases which refer to things which can be located on a chest X-ray, or confirmed not to be present.

If the report is in a language other than English, provide an English translation of each sentence and phrase in the fields "orig_en" and "new_en".

Code Snippet C.3: One of the in-context examples provided to GPT-4 for extracting negative finding phrases. Given the 'findings_text', GPT-4 outputs the 'parsed_report'.

```

"findings_text": "RX tórax posteroanterior: Impresión diagnóstica: Sin hallazgos patológicos para la edad del paciente.",
"parsed_report":
[
  {
    "orig": "RX tórax posteroanterior:",
    "orig_en": "Chest X-ray posteroanterior:",
    "new": [""],
    "new_en": []
  },
  {
    "orig": "Impresión diagnóstica:",
    "orig_en": "Diagnostic impression:",
    "new": [""],
    "new_en": []
  },
  {
    "orig": "Sin hallazgos patológicos para la edad del paciente.",
    "orig_en": "No pathological findings for the patient's age.",
    "new": ["Sin hallazgos patológicos para la edad del paciente.|non_finding"],
    "new_en": ["No pathological findings for the patient's age.|non_finding"]
  }
]

```

D Progression status

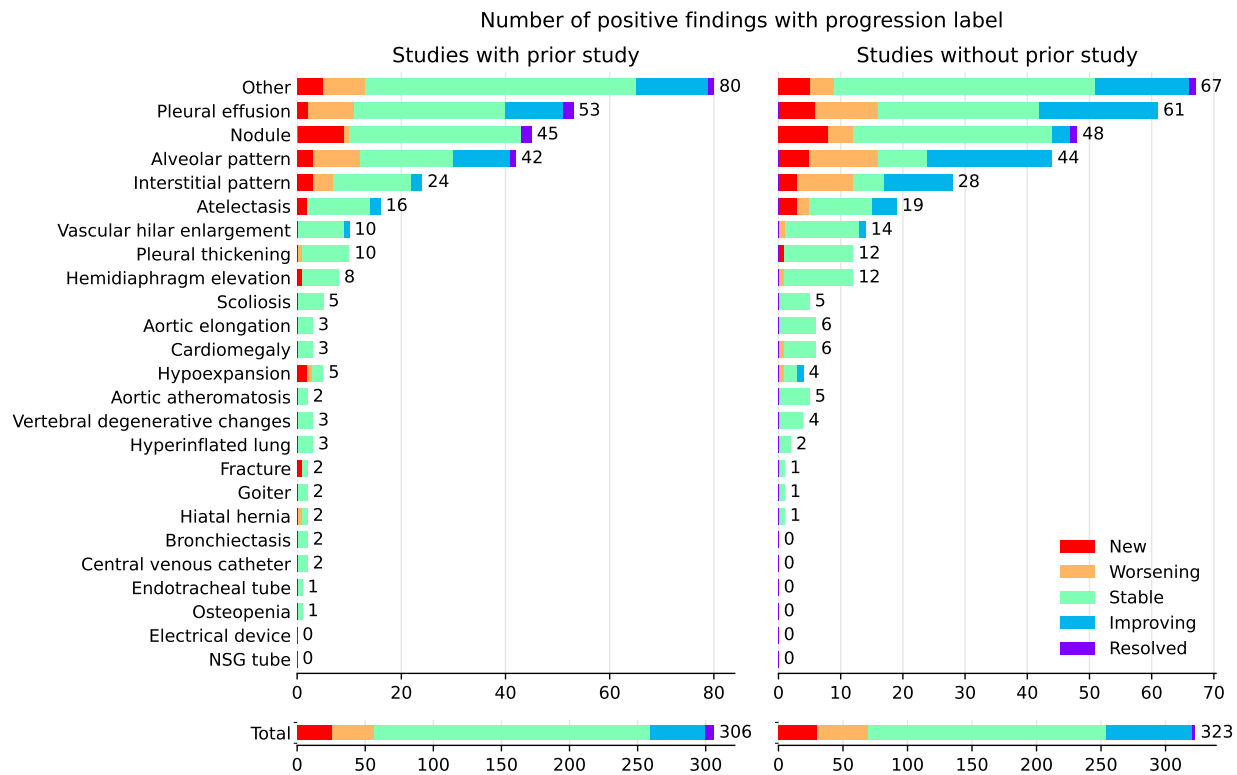


Figure D.1: Distribution of progression statuses across finding categories, for studies with and without prior studies available.

E Location labels

Table E.1: Distribution of location labels.

2691 images, 6588 boxes	(continued)
<ul style="list-style-type: none"> └ extracorporeal: 0 images, 0 boxes └ right: 845 images, 1207 boxes └ left: 645 images, 896 boxes └ bilateral: 419 images, 929 boxes └ cervical: 34 images, 39 boxes └ soft tissue: 231 images, 420 boxes <ul style="list-style-type: none"> └ subcutaneous: 8 images, 8 boxes └ axilar: 31 images, 39 boxes └ pectoral: 176 images, 358 boxes <ul style="list-style-type: none"> └ nipple: 67 images, 136 boxes └ bone: 445 images, 541 boxes <ul style="list-style-type: none"> └ shoulder: 90 images, 114 boxes <ul style="list-style-type: none"> └ acromioclavicular joint: 5 images, 8 boxes └ rotator cuff: 6 images, 7 boxes └ suprascapinous: 3 images, 4 boxes └ humerus: 71 images, 82 boxes <ul style="list-style-type: none"> └ humeral head: 28 images, 32 boxes └ humeral neck: 4 images, 4 boxes └ glenohumeral joint: 7 images, 8 boxes └ clavicle: 18 images, 18 boxes └ scapula: 10 images, 15 boxes └ costoesternal: 2 images, 3 boxes └ column: 146 images, 111 boxes <ul style="list-style-type: none"> └ intersomatic space: 6 images, 6 boxes └ dorsal vertebrae: 85 images, 54 boxes └ cervical vertebrae: 4 images, 4 boxes └ paravertebral: 20 images, 20 boxes └ rib: 165 images, 238 boxes <ul style="list-style-type: none"> └ anterior rib: 13 images, 15 boxes └ posterior rib: 29 images, 39 boxes └ rib cartilage: 4 images, 8 boxes └ hemithorax: 145 images, 232 boxes └ extrapleural: 3 images, 3 boxes └ extrapulmonary: 1 images, 1 boxes └ pleural: 471 images, 840 boxes └ subpleural: 3 images, 7 boxes └ fissure: 27 images, 27 boxes <ul style="list-style-type: none"> └ minor fissure: 17 images, 17 boxes └ major fissure: 3 images, 4 boxes └ lobar: 358 images, 505 boxes <ul style="list-style-type: none"> └ upper lobe: 191 images, 284 boxes <ul style="list-style-type: none"> └ left upper lobe: 82 images, 116 boxes <ul style="list-style-type: none"> └ lingula: 30 images, 34 boxes └ right upper lobe: 93 images, 125 boxes └ lower lobe: 101 images, 135 boxes <ul style="list-style-type: none"> └ left lower lobe: 45 images, 58 boxes └ right lower lobe: 43 images, 52 boxes └ middle lobe: 44 images, 52 boxes └ subsegmental: 41 images, 47 boxes └ bronchi: 91 images, 112 boxes └ peribronchi: 1 images, 2 boxes <ul style="list-style-type: none"> └ diffuse bilateral: 31 images, 61 boxes └ basal bilateral: 111 images, 194 boxes └ paratracheal: 23 images, 33 boxes └ airways: 191 images, 223 boxes <ul style="list-style-type: none"> └ tracheal: 104 images, 113 boxes └ bronchi: 91 images, 112 boxes 	
	<ul style="list-style-type: none"> └ lung field: 1485 images, 2698 boxes <ul style="list-style-type: none"> └ upper lung field: 297 images, 502 boxes <ul style="list-style-type: none"> └ upper lobe: 275 images, 461 boxes <ul style="list-style-type: none"> └ right upper lobe: 93 images, 125 boxes └ apical: 161 images, 289 boxes └ suprahilar: 10 images, 11 boxes └ middle lung field: 526 images, 934 boxes └ aortopulmonary window: 4 images, 3 boxes └ hilar: 448 images, 800 boxes <ul style="list-style-type: none"> └ pulmonary artery: 2 images, 1 boxes └ hilar bilateral: 19 images, 31 boxes └ perihilar: 73 images, 148 boxes └ minor fissure: 17 images, 17 boxes └ lower lung field: 916 images, 1325 boxes <ul style="list-style-type: none"> └ basal: 330 images, 460 boxes └ lower lobe: 101 images, 135 boxes <ul style="list-style-type: none"> └ left lower lobe: 45 images, 58 boxes └ right lower lobe: 43 images, 52 boxes └ middle lobe: 44 images, 52 boxes └ infrahilar: 54 images, 72 boxes └ lingula: 30 images, 34 boxes └ supradiaphragm: 2 images, 4 boxes └ diaphragm: 211 images, 261 boxes └ infradiaphragm: 34 images, 31 boxes └ cardiophrenic angle: 20 images, 24 boxes └ costophrenic angle: 196 images, 244 boxes <ul style="list-style-type: none"> └ right costophrenic angle: 56 images, 57 boxes └ left costophrenic angle: 85 images, 89 boxes └ bilateral costophrenic angle: 4 images, 10 boxes └ central: 86 images, 101 boxes └ mediastinum: 1120 images, 1594 boxes <ul style="list-style-type: none"> └ superior mediastinum: 143 images, 177 boxes <ul style="list-style-type: none"> └ carotid artery: 0 images, 0 boxes └ brachiocephalic veins: 1 images, 1 boxes └ supra aortic: 24 images, 30 boxes └ aortic button: 37 images, 38 boxes └ superior cave vein: 54 images, 62 boxes └ subclavian vein: 32 images, 44 boxes └ lower mediastinum: 559 images, 625 boxes <ul style="list-style-type: none"> └ anterior mediastinum: 2 images, 0 boxes <ul style="list-style-type: none"> └ thymus: 0 images, 0 boxes └ middle mediastinum: 494 images, 541 boxes <ul style="list-style-type: none"> └ cardiac: 493 images, 539 boxes <ul style="list-style-type: none"> └ coronary: 3 images, 3 boxes └ posterior mediastinum: 67 images, 78 boxes <ul style="list-style-type: none"> └ retrocardiac: 66 images, 77 boxes └ aortic: 620 images, 743 boxes └ esophageal: 3 images, 5 boxes └ paramediastinum: 4 images, 5 boxes └ paracardiac: 10 images, 15 boxes └ epigastric: 1 images, 1 boxes └ gastric chamber: 3 images, 3 boxes └ hypochondrium: 16 images, 23 boxes <ul style="list-style-type: none"> └ right hypochondrium: 13 images, 19 boxes <ul style="list-style-type: none"> └ gallbladder: 5 images, 7 boxes └ left hypochondrium: 3 images, 4 boxes